

Energy-Dependent Sticking Probabilities of Carbon Dioxide Isotopologues under Non-Equilibrium Gas-Surface Collision Conditions

Elizabeth A. Jamka, Francisco Lizano, Yuheng Luo, Christopher Kang, Rui Sun, and Steven J. Sibener*



Cite This: *J. Phys. Chem. C* 2025, 129, 15815–15824



Read Online

ACCESS |



Metrics & More

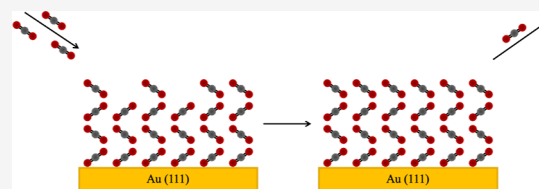


Article Recommendations



Supporting Information

ABSTRACT: The phenomenon of non-equilibrium gaseous condensation is not fully understood. Non-equilibrium gas-phase condensation is a dynamic process where gas molecules collide with an interface and lose energy through adiabatic or non-adiabatic interactions which dictate condensation behavior. This condensation process is governed by the kinetics of particle interactions, where the rate of condensation depends on multiple factors including incident kinematics, the interfacial phonon density of states, and the nature of



While non-equilibrium gas-phase condensation has been a topic of interest, there are still large gaps in the knowledge of the fundamental processes that govern such encounters, such as how the dissipation of energy affects energy accommodation with the surface. The outcome of such heterogeneous collision events are important for chemistry in the interstellar medium (ISM), where heterogeneous adsorption and subsequent reaction can occur, for example, on bare or ice-covered dust grains. Under favorable conditions, isotopes, due to their mass differences, can condense at differing rates, leading to isotopic abundance anomalies. This in turn leads to distinct isotopic signatures in the condensed phase, providing valuable insights into the chemical evolution of the interstellar medium. When studying isotopically selected species, insights into gas-surface energy transfer shed further light on real-world condensation events such as airframe icing in cold environments. In this paper we present a comprehensive molecular beam and molecular dynamics examination of the comparative sticking behavior for two CO₂ isotopologues, ¹²CO₂ and ¹³CO₂, at various energies. The experimental data span a range of energetic incident conditions and are obtained with the complementary use of King and Wells mass spectrometry combined with in situ reflection infrared spectroscopy (RAIRS) to monitor the probabilities of sticking on the respective condensed films of the CO₂ isotopologues.

INTRODUCTION

Gas-surface reactions mediated by adsorption processes play a significant role in both terrestrial and astrophysical environments where non-equilibrium interactions are dominant.^{1–5} Molecular beams enable the study of chemical dynamics under a range of conditions, including both gas phase and condensed phase interactions.⁵ The kinetic energy of molecular beam projectiles can be readily varied, aiding in the understanding of how molecules interact with the surface.^{4–6} This understanding is crucial for explaining rate-determining steps in many heterogeneous industrial and catalytic processes. In the context of astrophysical environments, such as the interstellar medium (ISM), understanding the dynamics of gas-phase molecules interacting with surface-bound species is essential to explain the molecular abundances and chemical complexity observed.^{7–10} Investigating spectra from the James Webb Telescope, it is apparent that many isotopologues are present in the ISM for many species including carbon monoxide and dioxide.^{11,12} ¹²CO₂/¹³CO₂ absorption peaks can serve as indicators of an interstellar ice's thermal history.^{11,13} Absorption spectra give information on the physical state and chemical composition of the CO₂ in ice mantles and the CO₂ peaks vary greatly depending on the physical and

chemical composition of the environment. There is particular interest in studying ¹³C isotopologues due to the ranging isotopic abundance ratio of ¹²C/¹³C in the Milky Way. Isotopic abundances of ¹²C/¹³C are also of interest as they may be telltales for signs of life.^{11,13,14} Additionally, determining the ratio between ¹²C and ¹³C is important for evolutionary models of the galaxy. A deeper understanding of how molecules and isotopes adhere to surfaces enhances our comprehension of non-equilibrium interactions in a variety of settings. Comparative condensation rates for isotopologues are also quite informative for probing the most fundamental contributions of energy dissipation, important for real-world technologies such as airframe performance in cold environments.

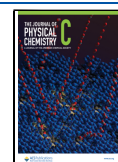
Solid-phase carbon dioxide (CO₂) is a prominent molecular species found within interstellar ices, young stellar objects, and

Received: June 15, 2025

Revised: August 7, 2025

Accepted: August 8, 2025

Published: August 13, 2025



comets, with abundances ranging from 10%–50% with respect to water.^{15–17} In molecular clouds, gas-phase atoms and molecules condense onto dust grains, forming molecular ices that are subject to physical and chemical processing from the astrophysical environment. These processes drive the formation of both novel and complex organic molecules, wherein reactions become more feasible upon the ice surface. The abundance of gaseous CO₂, however, is approximately 2 orders of magnitude less than its solid counterpart, as CO₂ is thought to form from the oxidation of surface-bound carbon monoxide, CO.¹⁸ Infrared (IR) measurements of pure CO₂ and CO₂-bearing ices indicate that the absorption profile is highly dependent on the physical and chemical environment provided by the ice, making CO₂ an important tracer of the thermal and chemical history of its surroundings.^{19–22}

In this study, we measure the sticking probabilities of gaseous ¹²CO₂ on ¹²CO₂ thin films of the same ice, with corresponding measurements also performed for the carbon-13 analog, as a function of incident kinematics. These probabilities were measured as a function of translational beam energy under ultrahigh-vacuum (UHV) conditions using the King and Wells method.²³ The growth of the ¹²CO₂ or ¹³CO₂ thin film was also monitored in real time with in situ reflection absorption infrared spectroscopy (RAIRS). We find that the sticking probability decreases as translational beam energy increases. Bonding in condensed CO₂ films is well-understood, including spectroscopic signatures for crystalline versus amorphous films.^{24–29} The CO₂ adsorption energy on a clean gold surface is reported to be 29, 31, and 33 meV on top, bridge, and hollow sites, respectively,²⁴ while the CO₂ on solid CO₂ binding energy is 231 meV.²⁵ Molecular dynamics (MD) simulations produce sticking probability values and behavior trending with our gas-surface scattering experiments, allowing us to investigate how increasing translational beam energy impacts the energy accommodation and adsorption of gaseous incident particles onto a thin ice film.

This work provides insight on the adsorption behavior of pure ¹²CO₂ under specific translational beam energy, flux, and film thickness conditions. Our precision molecular beam scattering instrument sheds further light on chemistry in the ISM through laboratory-based measurements. Moreover, such understanding of the sticking probability of ¹²CO₂ can further the development of astrophysical models that seek to explain molecular abundances seen in molecular clouds and young stellar bodies. The results also further understanding of gaseous condensation under non-equilibrium conditions, as seen in low-temperature aircraft aerodynamics.

EXPERIMENTAL METHODS

All experiments were performed with a molecular beam scattering instrument that has been discussed in detail in previous papers.^{26–28} This instrument consists of a UHV chamber with base pressures of 10^{–10} Torr connected to a triply differentially pumped molecular beamline. The main chamber has a helium closed-cycle refrigerator for cooling the sample with added vibrational isolation (Advanced Research Systems) which facilitates precise and accurate temperature control of a gold single crystal, Au(111), with temperatures spanning in these experiments between 30 and 750 K. All experiments performed allowed the Au(111) crystal to be exposed to the beam at a normal incidence while being monitored in real time with in situ reflection absorption infrared spectroscopy (RAIRS). Gas scattering was monitored

using a residual gas analyzer (RGA) and translational velocities were monitored by time-of-flight (TOF) methods using a quadrupole mass spectrometer.

¹²CO₂ (Air Gas, UHP) and ¹³CO₂ (Cambridge Isotopes) were independently dosed onto the Au(111) sample via molecular beam deposition at 30 to 31 K surface temperature. All molecular beams were produced by expanding either a 1% ¹²CO₂ in helium or 1% ¹³CO₂ in helium at backing pressures of 200 PSI through a 30 μm molybdenum pinhole. The metal nozzle was resistively heated from 300 to 900 K which resulted in beam velocities ranging from 1520 to 2650 m/s; time-of-flight FWHM widths spanned ca. 10% across this range corresponding to energy FWHM widths of 14 to 30%.

All infrared spectra were taken with a Nicolet 6700 infrared spectrometer using p-polarized incident IR radiation with a 75-degree incident angle from the Au(111) substrate. A liquid nitrogen-cooled mercury cadmium telluride (MCT/A) detector was used. All of the presented RAIRS spectra were obtained by collecting 200 scans with 2 cm^{–1} resolution. A clean Au(111) sample was used as a background reference. The RAIRS spectra were analyzed using multipeak Gaussian fitting atop cubic baselines to determine peak areas of individual IR peaks (Igor Pro8). The flux of the beam was determined for CO₂ by measuring the pressure changes with a nude Bayard-Alpert ion gauge calibrated to N₂ for a neat beam entering the chamber.²⁹ Flux was then calculated considering the relative gauge sensitivity, the spot size of the beam on the crystal, and the chamber pumping speed. The same beam was then used to determine the conversion to CO₂ film thickness by monitoring the growth on the substrate via RAIRS. At the surface temperatures of 30 K, deposited CO₂ forms a crystalline surface on the Au(111).^{30,31} The 2343 cm^{–1} asymmetric stretch (ν_3) was monitored as a function of time for ¹²CO₂ and 2277 cm^{–1} asymmetric stretch (ν_3) for ¹³CO₂. A calibration curve was used to determine the relationship between flux versus peak area. Assuming one monolayer (ML) equals 1 × 10¹⁵ molecules cm^{–2}, the peak areas were converted to layers. The initial thickness of CO₂ film for all experiments ranged from 12 to 15 layers depending on changes in the incident flux.

The sticking probabilities were determined by the King and Wells technique.^{23,28,32} These sticking probabilities were determined via eq 1, where an RGA out of line with the beam is used to monitor the pressures at different stages of the experiment, Figure 1. P_1 monitors the background signal of the main chamber, P_2 measures the indirect flux where a rotating flag is in front of the crystal, effectively blocking the beam from interacting with the surface. P_3 is when the flag is removed from the beam path, allowing the beam to interact with the surface and the molecules to stick. Each P region was collected over roughly a 320 s time period and the final value used in eq 1 was determined by averaging at least 75% of the collected points in each region. All King and Wells measurements were performed at 30–31 K surface temperature unless otherwise noted. IR spectra were taken before and after the King and Wells experiment to monitor the growth of the condensate on the underlying gold surface.

$$S = \frac{P_2 - P_3}{P_2 - P_1} \quad (1)$$

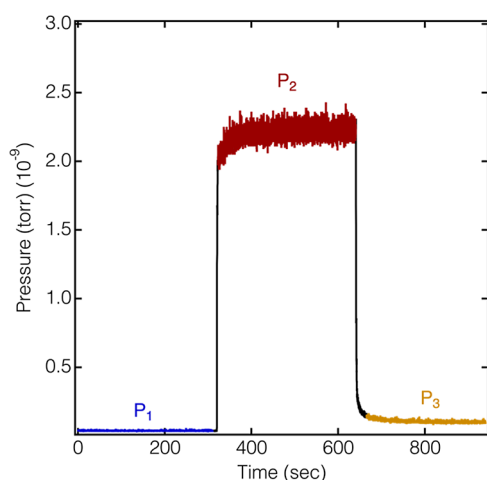


Figure 1. CO₂ signal ($m/z = 44$) monitored with RGA during a King and Wells experiment on a CO₂ surface at 30 K. P_1 (blue) in the background pressure of the chamber before the CO₂ beam is introduced, P_2 (red) is the CO₂ beam entering the chamber but a flag is blocking the beam from the surface, and P_3 (gold) is the initial CO₂ interacting with the surface after the flag has been moved.

COMPUTATIONAL METHODS

The potential energy function for both CO₂ gas and surface is given by

$$V = V_{\text{CO}_2(\text{b})} + V_{\text{CO}_2(\text{nb})} \quad (2)$$

where $V_{\text{CO}_2(\text{b})}$ is the bonded CO₂ potential and $V_{\text{CO}_2(\text{nb})}$ are the non-bonded CO₂ potential. The bond CO₂ potential ($V_{\text{CO}_2(\text{b})}$) is characterized by harmonic oscillations of carbon–oxygen (C–O) bonds and bending of the O–C–O angle

$$V_{\text{b}(r_{ij})} = \frac{1}{2}k_{\text{C-O}}(r_{ij} - b_{\text{C-O}})^2 \quad (3)$$

$$V_{\text{a}(\theta_{ijk})} = \frac{1}{2}k_{\text{O-C-O}}(\theta_{ijk} - \theta_{\text{C-C-C}})^2 \quad (4)$$

The non-bonded CO₂ potential ($V_{\text{CO}_2(\text{nb})}$) accounts for the van der Waals and Coulomb interactions between CO₂ molecules. van der Waals interactions are modeled with a 6–12 Lennard-Jones (L-J) potential of the following form

$$V_{\text{LJ}(r_{ij})} = 4\epsilon_{ij} \left[\left(\frac{\sigma_{ij}}{r_{ij}} \right)^{12} - \left(\frac{\sigma_{ij}}{r_{ij}} \right)^6 \right], \quad r_{ij} \leq 12 \text{ \AA} \quad (5)$$

where the ϵ_{ij} and σ_{ij} are the depth of the potential energy well and the equilibrium distance, respectively, and r_{ij} is the distance between atom i and atom j . The L-J (6–12) parameters for the different atom pair (C–O) are determined using Lorentz–Berthelot rules^{33,34}

$$\epsilon_{ij} = \sqrt{\epsilon_i \times \epsilon_j} \quad (6)$$

$$\sigma_{ij} = \frac{\sigma_i + \sigma_j}{2} \quad (7)$$

The Coulomb interactions are given by

$$V_{\text{c}(r_{ij})} = \frac{q_i q_j}{4\pi\epsilon_0 r_{ij}} \quad (8)$$

where q_i and q_j denote the partial charges of atom i and atom j , and ϵ_0 is the vacuum permittivity.

The force parameters used in this study are acquired from the flexible version of the Transferable Potentials for Phase Equilibria (TraPPE-flex) force field^{35,36} and summarized in Table 1.

Table 1. TraPPE-flex Force Field Parameters

bonded parameters		non-bonded parameters	
$b_{\text{C-O}}$ (Å)	1.16	$\epsilon_{\text{C-C}}$ (kJ/mol)	0.22449
$k_{\text{C-O}}$ (kJ/(mol·nm ²))	8.63×10^5	$\epsilon_{\text{O-O}}$ (kJ/mol)	0.65685
$\theta_{\text{O-C-O}}$ (°)	180.00	$\sigma_{\text{C-C}}$ (Å)	2.800
$k_{\text{O-C-O}}$ (kJ/(mol·rad ²))	468.92	$\sigma_{\text{O-O}}$ (Å)	3.050
		q_{C}	+0.70
		q_{O}	−0.35

The initial sampling of the ¹²CO₂ and ¹³CO₂ gas molecules was carried out using the chemical dynamics program VENUS³⁷ to replicate the experimental conditions. Four distinct translational energies were assigned to the CO₂ molecules: 537.5 meV, 1061.8, 1303.2, and 1553.4 meV, with each paired to a vibrational temperature (302.8, 600.5, 748.0, and 905.5 K, respectively) to match the experimental distributions. Vibrational energies were sampled from a Boltzmann distribution at these temperatures, while no initial rotational excitation was applied in any of the sampling sets.

The initial sampling of the ¹²CO₂ and ¹³CO₂ surface was carried out using GROMACS (Version 2023.2).³⁸ The CO₂ supercell was constructed with the VESTA (Version 3.90.1a)³⁹ visualization software and placed at the bottom of a periodic simulation box with dimensions approximately $5.65 \times 5.65 \times 400$ nm³. As shown in Figure 2, each layer of the surface contained 200 CO₂ molecules, and the surface used in our simulations consisted of nine such layers. The top layer was designated as the TOP layer, the middle four layers as the MID layers, and the bottom four layers as the BOT layers. The z-dimension of the simulation box was intentionally extended to prevent any artificial interactions between periodic images along the surface normal direction. The CO₂ surface is equilibrated by standard procedure. First, 5000 steps of steepest descent minimization were performed. This was followed by a 25 ns equilibration under the NVT ensemble with a 1 fs time step. The system temperature was maintained at 30 K using the V-rescale thermostat,⁴⁰ applied to the CO₂ surface with a coupling time constant of 0.1 ps. A further 25 ns simulation was carried out with the same 1 fs time step, and snapshots were saved every 2500 steps to build a surface configuration library for use in gas-surface collision simulations.

At the start of each trajectory, one CO₂ gas molecule (sampled by VENUS) was positioned approximately 25 Å above the CO₂ surface (sampled by GROMACS) with randomized molecular orientation and directed toward the surface. The incident angle, θ_1 , defined as the angle between the initial velocity vector of the gas molecule and the surface normal, was fixed at 0° in this study. The landing position of the gas molecule was randomly sampled across the entire surface supercell. A total of 1000 independent trajectories were simulated at each of the four translational energies (537.5 meV, 1061.8, 1303.2, and 1553.4 meV) with two isotopologues surfaces of ¹²CO₂ and ¹³CO₂. Trajectories were integrated using the leapfrog algorithm⁴¹ in GROMACS with a time step

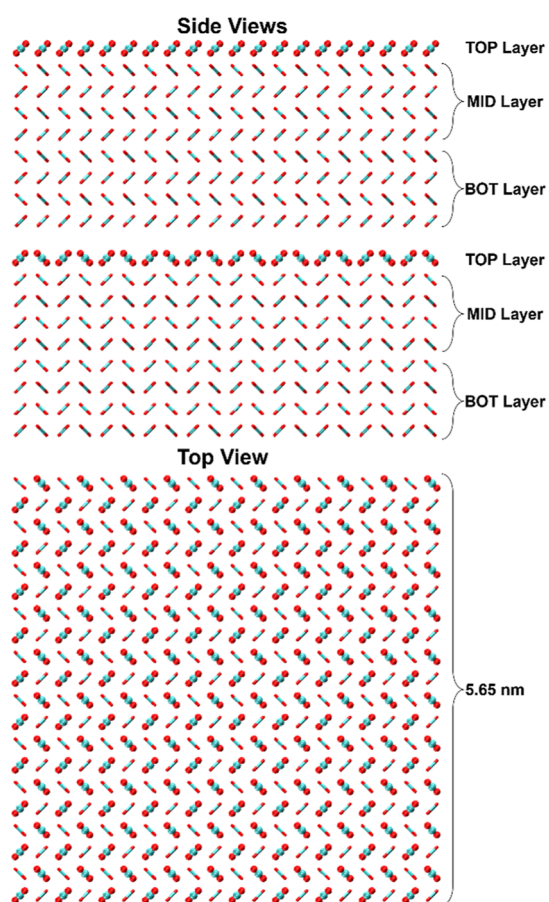


Figure 2. Structure of a perfect CO₂ surface. Ball-and-stick models represent the TOP layer; lines indicate the MID and BOT layers.

of 1 fs. Here we note the thermostat was only applied to the BOT layer, indirectly maintaining the CO₂ surface temperature

at 30 K. This setup was to mimic the controlled thermal conditions of the experimental setup and to mitigate potential artifacts introduced by thermostat that directly influence the collision dynamics. A trajectory was terminated either when the vertical distance between the gas molecule's center and the surface exceeded 50 Å following collision, or when the total simulation time reached 0.1 ns. Justification of the maximum time of simulation will be provided in the [Results and Discussion](#) section.

All simulations described above involved single-collision events between an individual CO₂ gas molecule and a perfectly smooth CO₂ surface. In addition, we performed supplementary tests to investigate conditions potentially closer to the experiment. These included: (1) simulations of 100 sequential collisions, where 100 ¹²CO₂ gas molecules consecutively impacted a small, square region (2.26 nm × 2.26 nm) at the center of a perfect ¹²CO₂ surface; (2) single-collision simulations with a defective ¹²CO₂ surface (DEF), where half of the molecules (100 ¹²CO₂ molecules) removed from the TOP layer; and (3) single-collision simulations with stepped, uneven ¹²CO₂ surfaces, where the TOP layer was reconstructed into two-step and four-step configurations, labeled STEP2 and STEP4, respectively. The structures of DEF, STEP2, and STEP4 surfaces are shown in [Figure 3](#).

RESULTS AND DISCUSSION

Experimental Results. The sticking probabilities of ¹²CO₂ on ¹²CO₂ ice (red circles) and its isotopologue, ¹³CO₂ on ¹³CO₂ ice (blue squares) as a function of energy are shown in [Figure 4](#). The sticking probability is close to unity at low incident energies and decreases to 0.88 as incident energies increase for both isotopologues. In order for physisorption trapping to occur, CO₂ molecules need to lose sufficient initial kinetic energy when they collide with the surface.^{42,43} If the energy loss is not sufficient, the molecule simply bounces off inelastically, as addressed in the corresponding MD simu-

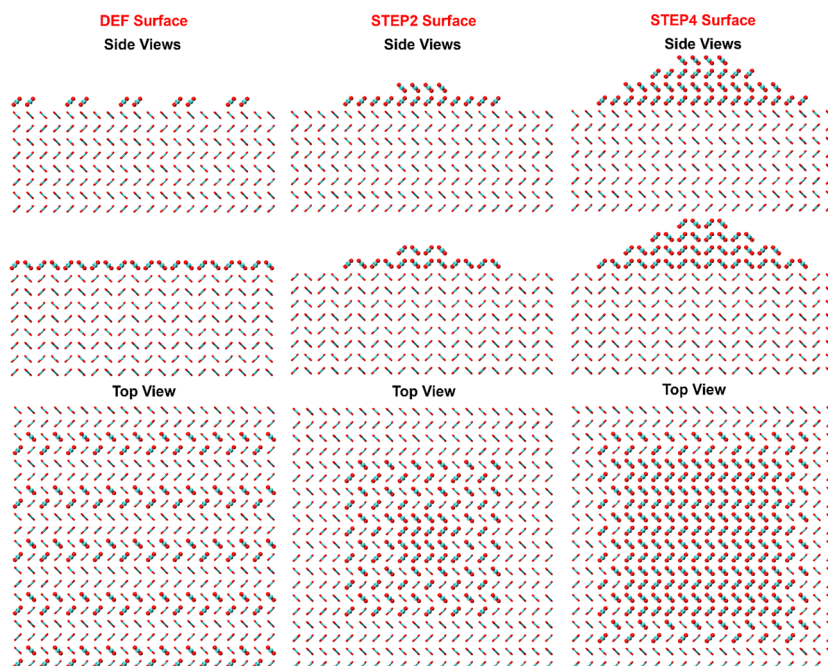


Figure 3. Structure of a DEF, STEP2, and STEP4 CO₂ surface. Ball-and-stick models represent the modified TOP layer; lines indicate the MID and BOT layers.

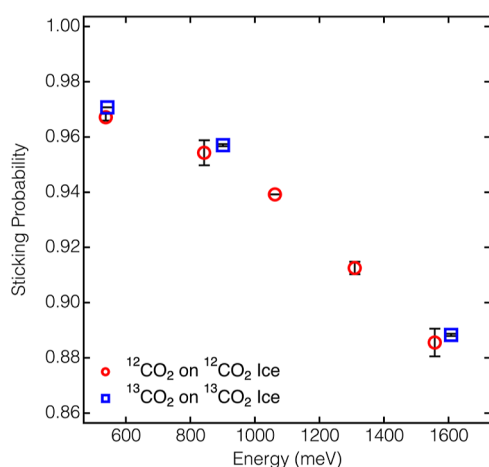


Figure 4. Sticking probability of $^{12}\text{CO}_2$ on a film of $^{12}\text{CO}_2$ (red open circles) and $^{13}\text{CO}_2$ on a film of $^{13}\text{CO}_2$ (blue open squares) at 30 K surface temperature. The sticking probability decreases with increasing energy. Error bars represent the standard deviation of at least three measurements on different days.

lations. The sticking probability decreases as the incident energy increases, since more energy must be lost during the initial encounter for the molecule to adhere. There was little difference in the sticking probabilities between the $^{12}\text{CO}_2$ and $^{13}\text{CO}_2$ projectiles, which suggests similar energy accommodation behavior.^{35,36}

The sticking probability can be modeled using a simplified representation of the interaction, such as a cube model.^{44,45} In this picture, an incident particle of mass m with incident energy E_i interacts with a surface of mass M and an attractive potential with a well of depth ϵ . In order for the incident particle to remain at the surface, the fraction of the incidence energy lost must be greater than $\frac{E_i}{E_i + \epsilon}$, and one can predict a sticking probability dependent on some critical energy E_c where the amount of energy lost exceeds $\frac{E_i}{E_i + \epsilon}$. Such behavior is modeled through a Fermi-like function in eq 9, as the trapping behavior mimics the density of states form predicted by the Fermi function.⁴⁶

$$\beta(E_i, T_s) = \frac{1}{\exp\left[\frac{E_i - E_c}{xT_s^{1/2}}\right] + 1} \quad (9)$$

Here, T_s is the surface temperature, and x is an adjustable parameter.⁴⁶ Employing eq 9, a nonlinear least-squares analysis is used to fit the function, treating x and E_c as optimizable parameters. For the $^{12}\text{CO}_2$ on $^{12}\text{CO}_2$ fit, we found that the model was optimized with $x = 134.39 \pm 4.56 \text{ meV}\cdot\text{K}^{-1/2}$ and $E_c = 3058.24 \pm 60.01 \text{ meV}$, and the $^{13}\text{CO}_2$ on $^{13}\text{CO}_2$ fit was optimized with $x = 130.52 \pm 6.12 \text{ meV}\cdot\text{K}^{-1/2}$ and $E_c = 3092.00 \pm 78.96 \text{ meV}$. The results of the fit are shown in Figure 5, utilizing the fact that the molecular beam is normal to the surface. The fit from eq 9 is in good agreement with the experimental molecular beam results, as seen in Figure 5a. Within the energy range of the experiment (550 meV–1650 meV), there are no significant differences seen in the calculated sticking probabilities for the two isotopologues as seen in Figure 5a (note that this simple model suggests a very small systematic difference in isotopologue sticking in which $^{13}\text{CO}_2$ has a slightly higher sticking probability due to more efficient energy accommodation in the heavier $^{13}\text{CO}_2$ thin film). The trendline was then extended to lower (0 meV) and higher (8000 meV) energy values than the experimental data, in order to better investigate the behavior of the sticking probabilities at both extremes (Figure 5b). The sticking probabilities of both isotopologues is below unity at 0 meV, which is in agreement with previous results.⁴⁷ The $^{12}\text{CO}_2$ trendline also intersects the $^{13}\text{CO}_2$ trendline at approximately 4000 meV, predicting a higher sticking probability for $^{12}\text{CO}_2$ on $^{12}\text{CO}_2$ at higher energies. Eventually, both isotopologues tend toward a sticking probability of 0 at high incident energies. This behavior aligns with the assumptions of the model since now the incident particles have too much energy to lose in order to remain at the surface. It has been well-defined that the use of $^{12}\text{CO}_2$ and $^{13}\text{CO}_2$ have been used in astrochemistry as thermal tracers to determine the history of interstellar grains and that the ratio of $^{12}\text{CO}_2/^{13}\text{CO}_2$ varies throughout space.^{11,13,14} The energy range used in the hard cube model in Figure 5b was chosen to give an overall view of sticking versus incident energy covering a very wide range of incident kinematics. The low end is relevant to the ISM, whereas the upper values give insight into the inhibition of sticking at high energies.

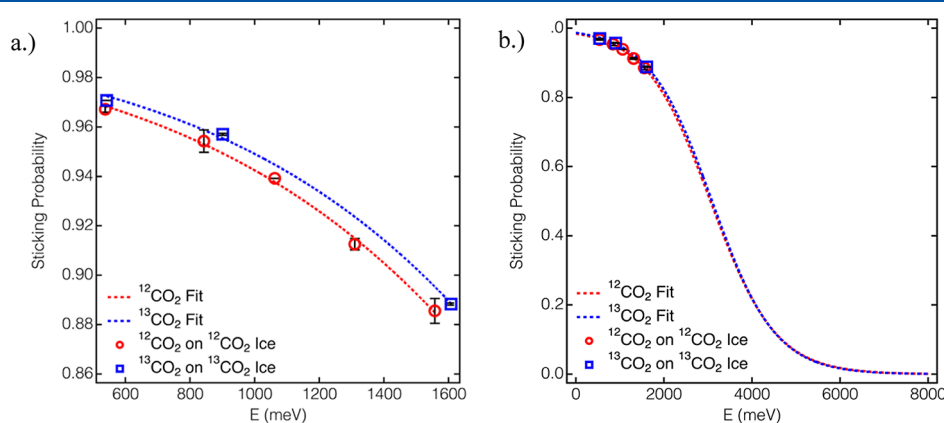


Figure 5. (a) Fitted sticking curve (dotted lines) for both $^{12}\text{CO}_2$ (red) and $^{13}\text{CO}_2$ (blue) versus energy, determined from the cube model represented by eq 9. Experimental data are the red ($^{12}\text{CO}_2$) and blue ($^{13}\text{CO}_2$) markers. (b) Same model used before with a larger energy range in order to see entire sticking probability from 1 to 0.

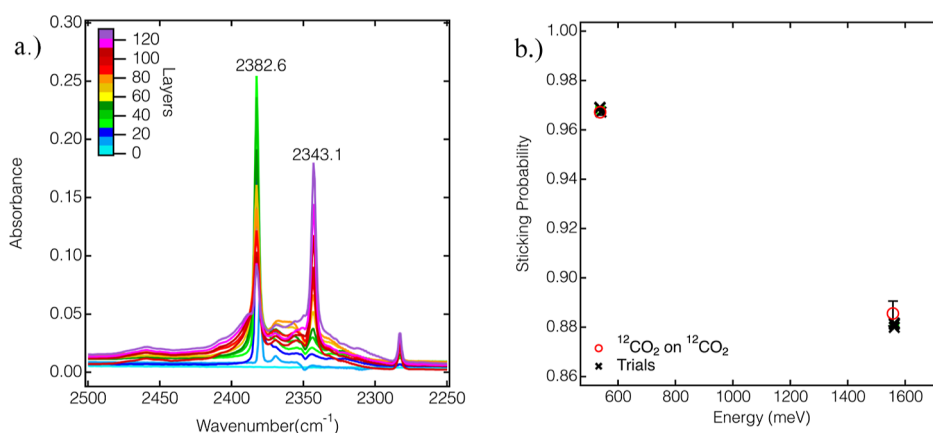


Figure 6. (a) RAIRS spectra of CO_2 ν_3 stretching mode at 2343.1 cm^{-1} and the LO peak at 2382.6 cm^{-1} . Spectra were taken at 200 scans with a resolution of 2 cm^{-1} and every 5 min over 50 min. As the dosing continues, the LO peak starts to decrease after 40 layers as the main CO_2 peak increases due to continual deposition. (b) The average sticking probabilities of multiple trials where the LO mode at 2382 cm^{-1} was present at various amplitudes. Triplicates at room and high temperature (black x) plotted against the energy.

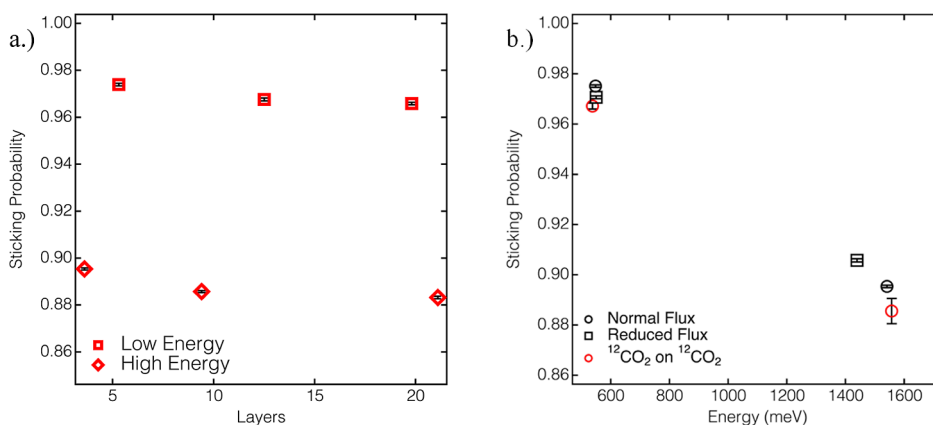


Figure 7. (a) Sticking coefficients of low energy (open squares) and high energy (open diamonds) versus layers of deposition. Layers ranged from 4.5 to 25 layers for both energies. (b) Sticking coefficients normal flux (black open circles), reduced (black open squares) versus energies of each beam, $^{12}\text{CO}_2$ on $^{12}\text{CO}_2$ sticking points at low and high energies (red open circles).

This model, however, is a hard cube model that does not account for other important contributions that influence sticking probability, such as the density of states of the film, the softness of the potential, or the internal modes of the molecule. Because these are known to influence sticking probabilities,^{48,49} more complex interactions need to be taken into consideration through the use of MD simulations later in the paper.

Infrared spectra were used to determine the initial ice thickness and to characterize the surface before and after King and Wells experiments. The CO_2 ν_3 asymmetric stretching mode (2343.1 cm^{-1}) was used to calculate the ice thickness. Another strong peak seen at 2382.6 cm^{-1} is consistent with the longitudinal optical (LO) phonon mode coupled to the ν_3 asymmetric stretch in crystalline CO_2 .^{50–52} The LO mode and ν_3 stretch are observed in Figure 6a. As the thickness of the CO_2 ice increases; the LO mode decreases over 50% while the ν_3 stretch increases. In order to determine if the LO mode has an effect on the sticking probability, triplicate trials were performed directly after each other at low and high molecular beam energies, Figure 6b. Throughout the trials the LO mode peak decreased between 30 and 50%, while the CO_2 peak at 2343.1 cm^{-1} continued to increase as film thickness increased.

The resulting sticking probabilities of each triplicate trial showed no changes in the sticking probability.

A number of conditions were additionally examined to determine their effect, if any, on sticking probabilities. We focused on the initial number of CO_2 ice layers and flux of CO_2 molecules in the beam. As shown in Figure 7a, the initial thickness of the deposited ice does not affect the sticking probability. Initial layers of less than 5 and greater than 20 layers were deposited on the surface and then the sticking probability was determined both at low energy (open square) and high energy (open diamond). After the initial 5 layers, there is very little difference in the sticking probability when comparing it to the red points; therefore, the thickness of the initial CO_2 ice deposition does not change how the incident beam of CO_2 behaves. When varying the flux of the beam, the primary flux used was set at $2.8 \times 10^{13} \text{ molecules cm}^{-2} \text{ s}^{-1}$ while the diminished beam was set at $1.6 \times 10^{13} \text{ molecules cm}^{-2} \text{ s}^{-1}$. When the flux was decreased, there was no change in sticking probability as in Figure 7b. It was determined that the sticking probability of $^{12}\text{CO}_2$ on $^{12}\text{CO}_2$ ice was independent of initial CO_2 ice thickness and magnitude of the flux of the molecular beam within the parameters examined.

Computational Results. To classify trajectories as sticking or non-sticking, the vertical position of the colliding CO_2

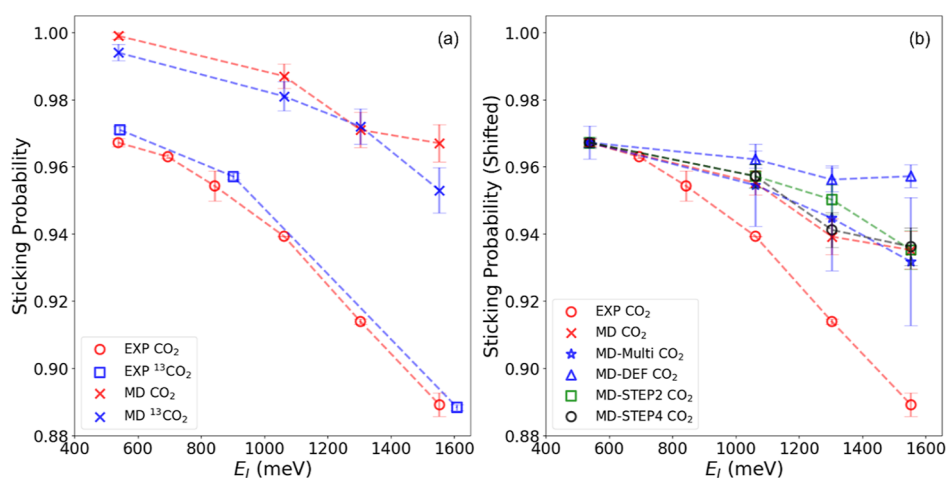


Figure 8. (a) Sticking probability of $^{12}\text{CO}_2$ on a film of $^{12}\text{CO}_2$ (red open circles: experiment, red crosses: molecular dynamics simulations) and $^{13}\text{CO}_2$ on a film of $^{13}\text{CO}_2$ (blue open squares: experiment, blue crosses: molecular dynamics simulations) at 30 K surface temperature. (b) Shifted sticking probabilities of CO_2 at 30 K surface temperature. The experimental sticking probability of CO_2 (red open circles) is compared with molecular dynamics (MD) simulations under various conditions: MD CO_2 (red crosses), MD-Multi CO_2 (blue stars), MD-DEF CO_2 (blue triangles), MD-STEP2 CO_2 (green squares), and MD-STEP4 CO_2 (black circles). The curves are shifted to align their lowest collision energy with the lowest experimental collision energy.

molecule relative to the surface was tracked throughout the simulation. Molecules remaining sticking to the surface by the end of the simulations are counted as sticking and molecules located at vertical distances greater than 50 Å from the surface are considered non-sticking. To examine whether those CO_2 that stuck to the surface after collision would fly off in longer simulations, 400 trajectories were extended to 0.4 μs and no desorption was observed. Therefore, for the purpose of ergodic sampling and analysis, we consider all the non-sticking CO_2 scatter off from the surface immediately (i.e., direct scattering) and only extended the simulations to 0.1 ns for the 1000 trajectories in the production run. As shown in Figure 8a, the MD simulation results agree qualitatively with the experiment, reproducing the decreasing trend of sticking probability with increasing incident energy. All translational energies and vibrational temperatures were chosen from the experimental values used. The translational energies were determined from the measured time-of-flight, rotational energies were frozen out as a result of supersonic seeded expansion of a beam at 10 K and considered negligible, and the vibrational temperatures from the temperature of the nozzle where the beam originated. Although MD simulations overestimate the sticking probabilities compared to the experimental data by 3–9% for the range of collision energy, this level of disagreement is in line with other gas-surface collision systems. For example, in the recent study of CH_4 or CD_4 gas colliding with a CH_4 or CD_4 surface, the reported disagreement between MD simulations and experimental results is as large as 6%.²⁹ In agreement with the experiment, simulations indicate the sticking probability is largely independent of the isotope effect of CO_2 .

To investigate the discrepancies between the MD simulations and experimental results, we conducted several additional simulations to mimic conditions (Figure 8) potentially closer to those of actual the experiment. In the sequential collision simulation, where 100 CO_2 gas molecules consecutively collide to a same small surface region (MD-Multi CO_2), previously sticking CO_2 molecules could be displaced from the surface by subsequent collisions. However, the overall sticking probability from these consecutive collisions remain within error bars of those from single collision. Here we note

that all 100 consecutive collisions take place in less than 100 ps, corresponding to a much larger particle density than the gas beam used in the experiment. Therefore, this simulation indicates cumulative collisions with the surface should not be a primary cause of the observed difference.

Simulations with the defective CO_2 surface (MD-DEF CO_2) showed higher sticking probabilities compared to the perfect surface. The presence of vacancies (holes) is likely to enhance attractive sites as incoming CO_2 molecules can interact simultaneously with both the first and second layers, thus enhancing surface sticking. As shown in Figure 3, the defects are clearly artificial and most likely an overestimate of the level of defects in the experimental surface, nonetheless, it gives a means to probe into the scattering dynamics of an extreme case. Considering the defective surface enhanced the sticking probability, it does contribute to what could explain the lower sticking probabilities observed experimentally. As an alternative to creating defective surfaces, two types of step surfaces are made (MD-STEP2 CO_2 and MD-STEP4 CO_2 , see Figure 3). These step surfaces contain a level of defects between the perfect surface (MD CO_2) and defective surface (MD-DEF CO_2) and resemble the “piling up” process of the experiment to some extent. For the perfect surface, all incident molecules approach perpendicular to the surface, but the presence of steps results in much more diverse collision geometries. However, simulations of these step surfaces yielded similar sticking probabilities. Therefore, surface defects are not likely to be the reason behind the difference between the experiments and the simulations.

Figure S1a presents a temperature analysis of different depths into the surface after a single CO_2 collision of the lowest energy (537.5 meV). The analysis reveals rapid heating of the TOP layer immediately following impact, with the temperature reaching nearly 35 K. The BOT layer, under the thermostat and located farthest from the collision site, remained stable with minimal level of fluctuations. The intermediate MID layers, functioned as thermal buffers, maintained temperatures between the TOP and BOT layers. This variation of temperature profile clearly demonstrates the existence of localized heating effects. A single collision of CO_2

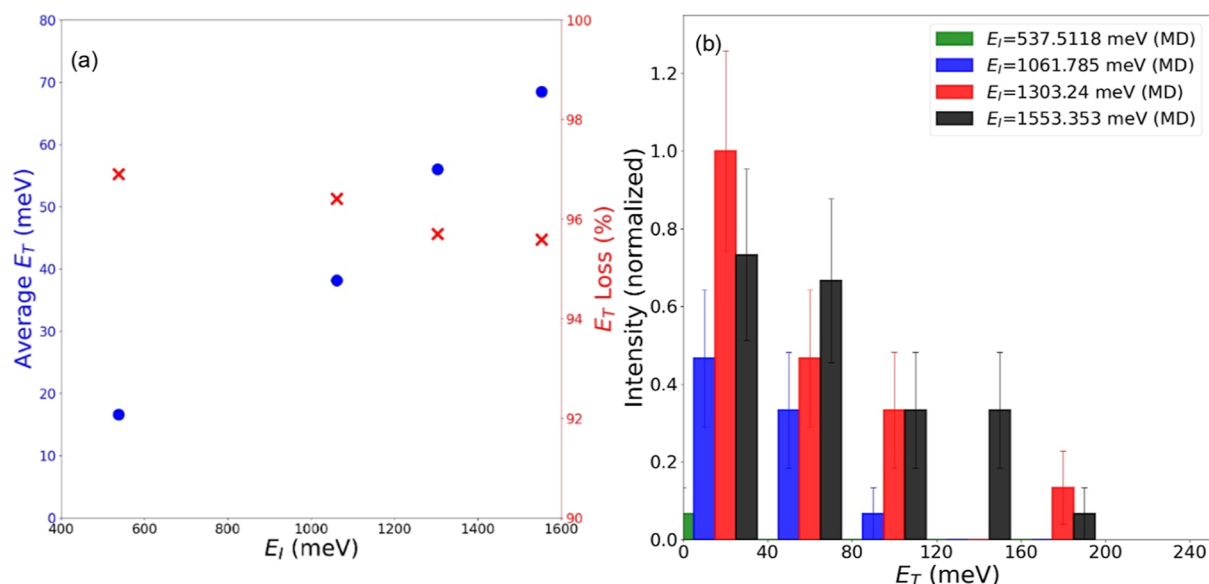


Figure 9. (a) Average translational energy (E_T , blue circles, left axis) of scattered CO_2 molecules and corresponding percentage energy loss (red crosses, right axis) as a function of incident collision energy (E_I). (b) Normalized intensity distributions of the translational energy (E_T) of scattered CO_2 molecules from MD simulations at incident collision energies (E_I) of 537.5 meV (green), 1061.8 meV (blue), 1303.2 meV (red), and 1553.4 meV (black). Although the histogram bars are visually offset to avoid overlapping, the peak positions for each data set fall within the same E_T bin range.

with a higher energy (1553.4 meV, Figure S1b) indicates a more significant localized heating effects, where the TOP layer temperature peaking around 38 K. To further explore the difference between MD simulations and experiments, we performed single-collision simulations at higher CO_2 surface temperatures (60 and 90 K). These simulations are designed to account for potential localized heating effects caused by gas-surface collisions, by both He (99%, carrier gas) and CO_2 (1%), under experimental conditions. Figure S1 shows that the effective temperature of the top layer is not likely to increase to above 60 K in the experiment even considering the collision of the carrier gas, nonetheless, these temperatures are selected to examine the upper limit of this phenomenon. As shown in Figure S2, increasing the surface temperature systematically reduces the gap between the simulation and experiment, particularly at low and intermediate collision energies. However, at higher collision energies, the difference remains noticeable, reaching approximately 3%.

Figure 9a presents the average translational energy (E_T) of non-sticking CO_2 molecules and the percentage of translational energy loss after collision with the CO_2 surface at various initial collision energies (E_I). While the value of average E_T increases with higher E_I , the percentage of energy loss decreases slightly as E_I increases, from approximately 98% at the lowest E_I to about 94% at the highest E_I . Energy loss remains high across all E_I , suggesting significant energy transfer during collisions, corroborating the localized heating phenomenon observed in the simulation. Figure 9b shows the normalized translational energy distributions for non-sticking CO_2 molecules at various initial collision energies. The distributions at all E_I have their primary peaks within the 0–25 or 25–50 meV bin, though the intensity and tail length differ. At 537.5 meV, only a single scattered trajectory was observed, whereas higher collision energies exhibit broader distributions with extended higher E_T tails.

DISCUSSION AND CONCLUSION

The sticking probabilities of $^{12}\text{CO}_2$ on $^{12}\text{CO}_2$ ice and $^{13}\text{CO}_2$ on $^{13}\text{CO}_2$ ice were determined using the King and Wells method to monitor sticking probabilities and RAIRS for thin film condensation and film growth. It was determined that as incident velocity and energy increased (up to 1600 meV), the sticking probability for both isotopologues monotonically decreased. No significant difference was found for the sticking probabilities of the two isotopologues as a function of energy within this energy range. These observations were confirmed both experimentally from detection of the reflected molecules via mass spectrometry, as well as theoretically from gas-surface chemical trajectory simulations and a simplified Baule model fit. The simplified Baule model approach showed $^{13}\text{CO}_2$ gas molecules on a $^{13}\text{CO}_2$ film to have a slightly higher sticking probability than the $^{12}\text{CO}_2$ isotopologue system until around 4000 meV. Multiple experimental variables were examined to determine if sticking probabilities were affected by incident beam velocity, thin film thickness, or flux magnitude of the molecular beam. For all of these variables, it was determined that they had no significant effect on the sticking probabilities. These results contribute to a deeper understanding of condensation of CO_2 gases under non-equilibrium conditions, which has important implications for reactions in terrestrial and astrophysical environments. The experimental conditions examined in this paper show a monotonic decrease in sticking probability of $^{12}\text{CO}_2$ on $^{12}\text{CO}_2$ ice and $^{13}\text{CO}_2$ on $^{13}\text{CO}_2$ ice as a function of incident translational energy as expected. No significant differences in the sticking probability between the two isotopologues were observed. This outcome suggests the need for further studies of isotope or isotopologue sticking involving a range of masses and molecular systems to generalize how different substrate density of states and incident particle kinematics can lead to differential condensation. Better understanding the energy-transfer dynamics of gaseous condensation under non-equilibrium conditions is

also important in other low temperature environments, such as for aircraft flight in cold environments. Additionally, the study of gaseous adsorption on ice surfaces has wider implications for fields such as thin film growth, heterogeneous catalysis, and other systems dependent upon gas adsorption. This work is pertinent for creating better astrophysical models of ice mantles and dust grains within the ISM in order to better understand chemical processes in the region.

■ ASSOCIATED CONTENT

SI Supporting Information

The Supporting Information is available free of charge at <https://pubs.acs.org/doi/10.1021/acs.jpcc.5c04151>.

Molecular dynamics simulations of temperature evolution for different surface layers during collisions plus molecular dynamics calculations of sticking probabilities at higher surface temperatures (PDF)

■ AUTHOR INFORMATION

Corresponding Author

Steven J. Sibener – *The James Frank Institute and Department of Chemistry, The University of Chicago, Chicago, Illinois 60637, United States*; orcid.org/0000-0002-5298-5484; Email: s-sibener@uchicago.edu

Authors

Elizabeth A. Jamka – *The James Frank Institute and Department of Chemistry, The University of Chicago, Chicago, Illinois 60637, United States*; orcid.org/0000-0002-6739-8872

Francisco Lizano – *The James Frank Institute and Department of Chemistry, The University of Chicago, Chicago, Illinois 60637, United States*; orcid.org/0000-0001-5568-5463

Yuheng Luo – *Department of Chemistry, The University of Hawaii Manoa, Honolulu, Hawaii 96822, United States*; orcid.org/0000-0002-3124-1179

Christopher Kang – *Department of Chemistry, The University of Hawaii Manoa, Honolulu, Hawaii 96822, United States*; orcid.org/0000-0002-9245-8101

Rui Sun – *Department of Chemistry, The University of Hawaii Manoa, Honolulu, Hawaii 96822, United States*; orcid.org/0000-0003-0638-1353

Complete contact information is available at: <https://pubs.acs.org/doi/10.1021/acs.jpcc.5c04151>

Notes

The authors declare no competing financial interest.

■ ACKNOWLEDGMENTS

The authors gratefully acknowledge funding from the Air Force Office of Scientific Research Grants FA9550-24-1-0338, with focus on the dynamics of energetic gas-surface interactions, FA9550-20-1-0351 with focus on ice interactions at interfaces, and support for instrumentation from the AFOSR-DURIP program Grant FA9550-23-1-0528. The National Science Foundation, with focus on interfacial chemical kinetics, is also gratefully acknowledged via Grant CHE-2313365, as well as infrastructure support from the NSF-Materials Research Science and Engineering Center at the University of Chicago, MRSEC Grant DMR-2011854. The authors also thank the Information and Technology Services (ITS) from the

University of Hawai'i, Manoa for the computational resources that enabled the simulations for this study.

■ REFERENCES

- (1) Hama, T.; Watanabe, N. Surface Processes on Interstellar Amorphous Solid Water: Adsorption, Diffusion, Tunneling Reactions, and Nuclear-Spin Conversion. *Chem. Rev.* **2013**, *113*, 8783–8839.
- (2) Burke, D. J.; Brown, W. A. Ice in Space: Surface Science Investigations of the Thermal Desorption of Model Interstellar Ices on Dust Grain Analogue Surfaces. *Phys. Chem. Chem. Phys.* **2010**, *12*, 5947–5969.
- (3) Watson, W. D. Interstellar Molecule Reactions. *Rev. Mod. Phys.* **1976**, *48* (4), 513–553.
- (4) Roessler, K. Non-Equilibrium Chemistry in Space. *Nucl. Instrum. Methods Phys. Res., Sect. B* **1992**, *65* (1–4), 55–66.
- (5) Kleyn, A. W. Molecular Beams and Chemical Dynamics at Surfaces. *Chem. Soc. Rev.* **2003**, *32* (2), 87–95.
- (6) Large, T. A. L.; Nesbitt, D. J. Quantum-State-Resolved Scattering of OCS at the Gas-Liquid Interface: Hyperthermal versus Thermal Vibrational Equilibration Dynamics in Polyatomics. *J. Phys. Chem. C* **2023**, *127* (37), 18586–18597.
- (7) Wilson, T. L.; Matteucci, F. Abundances in the Interstellar Medium. *Astron. Astrophys.* **1992**, *4* (1), 1–33.
- (8) Watanabe, N.; Kouchi, A. Ice Surface Reactions: A Key to Chemical Evolution in Space. *Prog. Surf. Sci.* **2008**, *83* (10–12), 439–489.
- (9) Polanyi, J. C. Nonequilibrium Processes. *Appl. Opt.* **1971**, *10* (8), 1717–1724.
- (10) Borengasser, Q.; Hager, T.; Kanaherachchi, A.; Troya, D.; Broderick, B. M. Conformer-Specific Desorption in Propanol Ices Probed by Chirped-Pulse Millimeter-Wave Rotational Spectroscopy. *J. Phys. Chem. Lett.* **2023**, *14* (29), 6550–6555.
- (11) McClure, M. K.; Rocha, W. R. M.; Pontoppidan, K. M.; Crouzet, N.; Chu, L. E. U.; Dartois, E.; Lamberts, T.; Noble, J. A.; Pendleton, Y. J.; Perotti, G.; et al. An Ice Age JWST Inventory of Dense Molecular Cloud Ices. *Nat. Astron.* **2023**, *7* (4), 431–443.
- (12) Howard, T.; Maheshwari, S.; Yeh, G. J.; Ganley, S. E.; Dodson, L. G. The 1.5 Mm Band of Cyanoacetylene as a Spectroscopic Target in Astrochemistry. *J. Phys. Chem. Lett.* **2025**, *16* (15), 3748–3753.
- (13) Brunken, N. G. C.; Rocha, W. R. M.; Dishoeck, E. F. V.; Gutermuth, R.; Tyagi, H.; Slavickinska, K.; Nazari, P.; Megeath, S. T.; Evans, N. J.; Narang, M.; et al. JWST Observations of 13CO₂ice: Tracing the Chemical Environment and Thermal History of Ices in Protostellar Envelopes. *Astron. Astrophys.* **2024**, 685.
- (14) Clayton, D. D.; Nittler, L. R. Astrophysics with Presolar Stardust. *Annu. Rev. Astron. Astrophys.* **2004**, *42* (1), 39–78.
- (15) Boonman, A. M. S.; Dishoeck, E. F. V.; Lahuis, F.; Doty, S. D. Gas-Phase CO toward Massive Protostars. *Astron. Astrophys.* **2003**, *399* (3), 1063–1072.
- (16) Gerakines, P. A.; Whittet, D. C. B.; Ehrenfreund, P.; Boogert, A. C. A.; Tielens, A. G. G. M.; Schutte, W. A.; Chiar, J. E.; Dishoeck, E. F. v.; Prusti, T.; Helmich, F. P.; et al. Observations of Solid Carbon Dioxide in Molecular Clouds with the Infrared Space Observatory. *Astrophys. J.* **1999**, *522* (1), 357–377.
- (17) Dishoeck, E. F. v.; Helmich, F. P.; Graauw, T. D.; Black, J. H.; Boogert, A. C. A.; Ehrenfreund, P.; Gerakines, P. A.; Lacy, J. H.; Millar, T. J.; Schutte, W. A.; et al. A Search for Interstellar Gas-Phase CO₂. Gas: Solid State Abundance Ratios. *Astron. Astrophys.* **1996**, *315*, L349–L352.
- (18) Bredehöft, J. H. CO₂: A Small Ubiquitous Molecule With a Lot of Astrochemical Debate Attached. *Front. Astron. Space Sci.* **2020**, *7*, 33.
- (19) Ehrenfreund, P.; Boogert, A. C. A.; Gerakines, P. A.; Tielens, A. G. G. M.; Dishoeck, E. F. v.; Ehrenfreund, P.; Boogert, A. C. A.; Gerakines, P. A.; Tielens, A. G. G. M.; Dishoeck, E. F. v. Infrared Spectroscopy of Interstellar Apolar Ice Analogs. *Astron. Astrophys.* **1997**, *328*, 649–669.

- (20) Isokoski, K.; Poteet, C. A.; Linnartz, H. Highly Resolved Infrared Spectra of Pure CO₂ Ice (15–75 K). *Astron. Astrophys.* **2013**, *555*, A85.
- (21) Broekhuizen, F. A. V.; Groot, I. M. N.; Fraser, H. J.; Dishoeck, E. F. V.; Schlemmer, S. Infrared Spectroscopy of Solid CO–CO₂ Mixtures and Layers. *Astron. Astrophys.* **2006**, *451* (2), 723–731.
- (22) He, J.; Emtiaz, S. M.; Boogert, A.; Vidali, G. The 12 CO 2 and 13 CO 2 Absorption Bands as Tracers of the Thermal History of Interstellar Icy Grain Mantles. *Astrophys. J.* **2018**, *869* (1), 41.
- (23) King, D. A.; Wells, M. G. Molecular Beam Investigation of Adsorption Kinetics On Bulk Metal Targets: Nitrogen On Tungsten. *Surf. Sci.* **1972**, *29*, 454–482.
- (24) Liu, X.; Sun, L.; Deng, W. Q. Theoretical Investigation of CO₂ Adsorption and Dissociation on Low Index Surfaces of Transition Metals. *J. Phys. Chem. C* **2018**, *122* (15), 8306–8314.
- (25) Sandford, S. A.; Allamandola, L. J. The Physical and Infrared Spectral Properties of CO₂ in Astrophysical Ice Analogs. *Astrophys. J.* **1990**, *355*, 357.
- (26) Gibson, K. D.; Killelea, D. R.; Yuan, H.; Becker, J. S.; Sibener, S. J. Determination of the Sticking Coefficient and Scattering Dynamics of Water on Ice Using Molecular Beam Techniques. *J. Chem. Phys.* **2011**, *134* (3), 034703.
- (27) Langlois, G. G.; Li, W.; Gibson, K. D.; Sibener, S. J. Capture of Hyperthermal CO₂ by Amorphous Water Ice via Molecular Embedding. *J. Phys. Chem. A* **2015**, *119* (50), 12238–12244.
- (28) Thompson, R. S.; Brann, M. R.; Sibener, S. J. Sticking Probability of High-Energy Methane on Crystalline, Amorphous, and Porous Amorphous Ice Films. *J. Phys. Chem. C* **2019**, *123* (29), 17855–17863.
- (29) Nakao, F. Determination of the Ionization Gauge Sensitivity Using the Relative Ionization Cross-Section. *Vacuum* **1975**, *25*, 431–435.
- (30) Ioppolo, S.; Noble, J. A.; Muiña, A. T.; Cuppen, H. M.; Coussan, S.; Redlich, B. Infrared Free-Electron Laser Irradiation of Carbon Dioxide Ice. *J. Mol. Spectrosc.* **2022**, *385*, 111601.
- (31) Weida, M. J.; Spherac, J. M.; Nesbitt, D. J. Sublimation Dynamics of CO₂ Thin Films: A High Resolution Diode Laser Study of Quantum State Resolved Sticking Coefficients. *J. Chem. Phys.* **1996**, *105* (2), 749–766.
- (32) Brann, M. R.; Hansknecht, S. P.; Ma, X.; Sibener, S. J. Differential Condensation of Methane Isotopologues Leading to Isotopic Enrichment under Non-Equilibrium Gas-Surface Collision Conditions. *J. Phys. Chem. A* **2021**, *125* (42), 9405–9413.
- (33) Berthelot, D. Sur Le Melange Des Gaz. *C. R. Chim.* **1898**, *126*, 15.
- (34) Lorentz, H. A. Ueber Die Anwendung Des Satzes Vom Virial in Der Kinetischen Theorie Der Gase. *Ann. Phys.* **1881**, *248*, 127–136.
- (35) Potoff, J. J.; Siepmann, J. I. Vapor–Liquid Equilibria of Mixtures Containing Alkanes, Carbon Dioxide, and Nitrogen. *AIChE J.* **2001**, *47* (7), 1676–1682.
- (36) Cao, H.; Cao, X.; Chen, J.; Zhao, X.; Ding, G.; Guo, D.; Liu, Y.; Li, H.; Bian, J. Molecular Dynamics Simulation of the Transport Properties and Condensation Mechanism of Carbon Dioxide. *J. Nat. Gas Sci. Eng.* **2022**, *105*, 104692.
- (37) Lourderaj, U.; Sun, R.; Kohale, S. C.; Barnes, G. L.; Jong, W. A. D.; Windus, T. L.; Hase, W. L. The VENUS/NWChem Software Package. Tight Coupling between Chemical Dynamics Simulations and Electronic Structure Theory. *Comput. Phys. Commun.* **2014**, *185* (3), 1074–1080.
- (38) Abraham, M. J.; Murtola, T.; Schulz, R.; Páll, S.; Smith, J. C.; Hess, B.; Lindahl, E. GROMACS: High Performance Molecular Simulations through Multi-Level Parallelism from Laptops to Supercomputers. *SoftwareX* **2015**, *1–2*, 19–25.
- (39) Momma, K.; Izumi, F. VESTA 3 for Three-Dimensional Visualization of Crystal, Volumetric and Morphology Data. *J. Appl. Crystallogr.* **2011**, *44* (6), 1272–1276.
- (40) Bussi, G.; Donadio, D.; Parrinello, M. Canonical Sampling through Velocity Rescaling. *J. Chem. Phys.* **2007**, *126* (1), 014101.
- (41) Gunsteren, W. F. V.; Berendsen, H. J. C. A Leap-Frog Algorithm for Stochastic Dynamics. *Mol. Simul.* **1988**, *1* (3), 173–185.
- (42) Sibener, S. J.; Lee, Y. T. The Internal and Translational Energy Dependence of Molecular Condensation Coefficients: SF₆ and CCl₄. *J. Chem. Phys.* **1994**, *101* (2), 1693–1703.
- (43) Park, G. B.; Krüger, B. C.; Borodin, D.; Kitsopoulos, T. N.; Wodtke, A. M. Fundamental Mechanisms for Molecular Energy Conversion and Chemical Reactions at Surfaces. *Prog. Phys.* **2019**, *82* (9), 096401.
- (44) Kao, C. L.; Carlsson, A.; Madix, R. J. Mass and Lattice Effects in Trapping: Ar, Kr, and Xe on Pt(1 1 1), Pd(1 1 1), and Ni(1 1 1). *Surf. Sci.* **2004**, *565* (1), 70–80.
- (45) Goodman, F. O. *Dynamics of Gas-Surface Scattering*; Elsevier Science, 2014.
- (46) Rettner, C. T.; Schweizer, E. K.; Mullins, C. B. Desorption and Trapping of Argon at a 2H–W(100) Surface and a Test of the Applicability of Detailed Balance to a Nonequilibrium System. *J. Chem. Phys.* **1989**, *90* (7), 3800–3813.
- (47) Gibson, K. D.; Luo, Y.; Kang, C.; Sun, R.; Sibener, S. J. The Initial Sticking of High Velocity Water onto Graphite under Non-Equilibrium Supersonic Flow Conditions. *J. Chem. Phys.* **2024**, *160* (19), 194705.
- (48) Hundt, P. M.; Bisson, R.; Beck, R. D. The Sticking Probability of D₂O-Water on Ice: Isotope Effects and the Influence of Vibrational Excitation. *J. Chem. Phys.* **2012**, *137* (7), 074701.
- (49) Krivchikov, A. I.; Stachowiak, P.; Pisarska, E.; Jezowski, A. Orientational Isotopic Effects in the Thermal Conductivity of CH₄/CD₄ Solid Solutions. *Low Temp. Phys.* **2007**, *33* (12), 1061–1067.
- (50) Smith, R. S.; Kay, B. D. Desorption Kinetics of Carbon Dioxide from a Graphene-Covered Pt(111) Surface. *J. Phys. Chem. A* **2019**, *123* (15), 3248–3254.
- (51) Jansen, C.; Juurlink, L. B. F. State-Resolved Studies of CO₂ Sticking to CO₂ Ice. *Front. Chem.* **2023**, *11*, 1250711.
- (52) Escribano, R. M.; Muñoz Caro, G. M.; Cruz-Diaz, G. A.; Rodríguez-Lazcano, Y.; Maté, B. Crystallization of CO₂ Ice and the Absence of Amorphous CO₂ Ice in Space. *Proc. Natl. Acad. Sci. U.S.A.* **2013**, *110* (32), 12899–12904.